УДК 550.34, 551.24, 550.394 DOI: https://doi.org/0.24028/gj.v48i2.350985

Application of machine learning methods to study the relationships between seismicity and geodynamic features of the Dnister Hydropower Complex

I.V. Brusak[1], O.A. Haidus[1], B.Ye. Kuplovskyi[2], 2026

[1]Lviv Polytechnic National University, Institute of Geodesy, Lviv, Ukraine
[2]Department of Seismicity of the Carpathian Region of the S. Subbotin Institute of Geophysics of National Academy of Sciences of Ukraine, Lviv, Ukraine
Received 28 January 2025

This study investigates the seismicity and recent geodynamic features of the Dnister Hydropower Complex in Ukraine, emphasizing the application of machine learning methods to analyze their interrelationships. The complex, situated in a seismically active transitional zone, is influenced by natural tectonic processes and anthropogenic activities, including the operations of the Dnister Hydroelectric Power Plant and active water level changes at the Dnister Reservoir. Data from digital seismic stations of the Carpathian Seismological Network, permanent Global Navigation Satellite System stations of GeoTerrace and SystemNet networks, as well as reservoir water level records of Dnister Reservoir, were collected and analyzed together. Machine learning algorithms, including Random Forest, Isolation Forest, and DBSCAN clustering, were employed to identify patterns and correlations between crustal deformations, water level fluctuations, and seismic events. Results reveal a significant association between water level changes — both short-term and long-term — and earthquake occurrences, suggesting that hydrological variations impact seismic activity. Geodynamic analysis indicates heterogeneous deformation patterns, with increased velocities in seismically active southwestern regions. Global Navigation Satellite System data shows velocities increasing by about 2 mm/year near the Dnister Hydropower Complex. Seismicity near the Dnister Hydropower Complex from 2012 to 2023 was characterized by peak earthquake years of 2014—2016 and 2022, each with over 100 events. The total seismic energy released increased from $\lg(\Sigma E)$=7.5 in 2012 to 10 in 2016, then steadily declined to 7 by 2023. The findings enhance understanding of the mechanisms of induced seismicity related to reservoir operations and provide valuable insights for risk assessment and mitigation strategies in hydroelectric regions. This integrated approach demonstrates the effectiveness of machine learning in deciphering complex geodynamic and seismic interactions in tectonically sensitive environments.

Key words: seismicity, recent geodynamics, reservoir-triggered seismicity, water level changes, Dnister Hydropower Complex, machine learning.

Introduction. Powered by the waters of the Dnister River, the Dnister Hydropower Complex is located at the junction of the Chernivtsi, Vinnytsia, and Khmelnytskyi regions. It is one of the most important energy facilities in Ukraine. It includes the Dnister Hydroelectric Power Plant (HPP), the Dnister Pumped Storage Power Plant (PSPP), and the

Citation: Brusak, I.V., Haidus O.A., & Kuplovskyi, B.Ye. (2026). Application of machine learning methods to study the relationships between seismicity and geodynamic features of the Dnister Hydropower Complex. *Geofizychnyi Zhurnal*, *48*(2), 60—76. https://doi.org/10.24028/gj.v48i2.350985.

Lower Dnister HPP. The facility relies on the Dnister main reservoir and a buffer reservoir situated between the Dnister and Lower Dnister HPPs. Construction commenced in 1973 with the Dnister HPP, followed by work on the Lower Dnister HPP in 1982. The ongoing construction of the Dnister PSPP underscores the importance of geodynamic and engineering monitoring across the entire region. It is evident that such a large-scale, prolonged construction project has a significant anthropogenic impact on the region. This influence is particularly pronounced given that the area of the Complex is seismically active and, according to Ukraine's seismic zoning, lies within the transitional zone between the intensity isoseisms VI and VII [DBN V.1.1-12:2014]. These factors considerably affect the region's geodynamic and seismic characteristics, which have been extensively studied in recent decades by various researchers [Brusak et al., 2022; Zyhar et al., 2023].

According to tectonic zoning, the Complex is located at the junction of the Dnister-Buh megablock of the Ukrainian Shield and the Volyn-Podillia and Moldavian Plates [Hurskyi, Kruglov, 2007], separated by the boundary of Vendian sedimentary deposits. The geological structure of the upper crust in this area includes two distinct structural levels: the upper level, composed of sedimentary and slightly volcanogenic-sedimentary deposits of the cover rock complex, and the lower level, represented by crystalline formations of the folded complex [State …, 2007]. The Podillia fault zone forms the southwestern boundary of the Ukrainian Shield and is oriented northwest. It is complicated by transverse faults with a northeastern strike, and is considered a series of low-amplitude faults that fragment the basement into small blocks. The Podillian Dnister region, due to its structural features, is a tectonic node within a rotational stress-release field, forming a «vortex» fault system [Sarnavski, Ovsiannikov, 2005]. Additionally, a fan-like system of intersecting arcuate fractures surrounds central-type structures and is expressed in the interblock zones. These are known as geoenergetic (or geodynamic) zones, which serve as areas of accumulation, transformation, and release of tectonic stress. Local earthquake epicenters are also associated with these zones.

The interrelationship between recent geodynamics and earthquakes has been studied by many researchers and remains unresolved. Tretyak and Romaniuk [2018] identified a stable correlation between the vertical deformations across Europe and manifestations of generalized seismicity. As a continuation of this work, less stable but still significant correlations were found between horizontal compression-extension of territories, derived from Global Navigation Satellite System (GNSS) data, and generalized seismicity. The verification of regional geodynamic models and identification of zones with potential seismic risk based on lithospheric dynamics, geophysical, and geodetic data is demonstrated in [Pospisil et al., 2019]. Kao et al. [2018] trace the relationship between earthquake moments and regional tectonic stress in western Canada and highlight tectonic deformation as the primary factor behind induced seismicity.

Recent studies focused specifically on the territory of the Complex indicate an increase in earthquake occurrences and the presence of induced seismic activity in the region. Some researchers attribute this to the construction of hydroengineering structures and the filling of the Dnister Reservoir basin [Sarnavski, Ovsiannikov, 2005; Savchyn, Pronyshyn, 2020]. Others examine the mechanisms of detected earthquakes around the Dnister HPP and determine the critical stress values (based on the Coulomb-Mohr theory) that lead to the breakdown of structural bonds and define optimal reservoir operation regimes. Zyhar et al. [2023] suggest that the highest density of earthquakes occurs in soils with an internal cohesion coefficient of C=0.2 MPa. The latest studies demonstrate a correlation between changes in reservoir water levels, regulated by the operation of the Dnister HPP, and the occurrence of earthquakes at depths of 2—3 km nearby [Tretyak et al., 2024b]. Such findings emphasize the importance of continuous monitoring of the technical condition of the Dnister HPP and the development of risk management strategies.

The aim of this study is to comprehensively examine the seismicity and geodynamics of the Complex, taking into account both natural and induced seismicity. To this end, data on earthquakes were collected from seismic stations in the region, current geodynamic features were assessed using permanent GNSS stations, data on reservoir water level fluctuations were obtained, and these results were analyzed using machine learning methods.

Methods and results. ***Recent geodynamic features of the region.*** At present, the most effective approach for assessing the contemporary geodynamics of large territories is to use data from permanent GNSS stations [Doskich et al., 2023; Naumowicz et al., 2024; Fazilova et al., 2025; Wu et al., 2025]. The geodynamics of the area during construction of the Dnister PSPP has also been evaluated through long-term GNSS campaigns [Sidorov et al., 2015; Savchyn, Pronyshyn, 2020]. The results over the past two decades indicate a redistribution of compression and extension zones in the region, induced by the large-scale construction of this hydraulic facility. However, these elastic deformations are not irreversible.

To identify and quantitatively assess the deformations of the Complex, multi-year GNSS data from 2019 to 2024 were utilized (from the GeoTerrace and System.NET networks) [Tretyak et al., 2024a]. The input consisted of daily 24-hour RINEX satellite files. The results were processed using the Bernese GNSS software package via the double-difference method. The daily solutions for all three coordinate components, with sub-centimeter accuracy, allowed the construction of multi-year time series. From these time series, the trend component was extracted, enabling the characterization of the stations' current spatial motions and, when processed collectively, the region's deformation.

The primary selection criteria for GNSS stations from the GeoTerrace and System.NET networks included the number of daily solutions, the duration and stability of station operations, as well as the geometric configuration and spatial coverage of the network. Eight permanent GNSS stations were selected, namely KLMN, NDNS, RALI, VINK, VINT, VOVK, VRBK, TULC, and YAMP. Most stations (KLMN, NDNS, VOVK, and partly VINT) demonstrated high data integrity (>80 %). However, in 2023, there was a significant decrease in data acquisition integrity and stability for RALI (59 %) and VRBK (58 %), which is attributed to the operational complications of CORS during the war. These challenges include blackouts, communication failures, electronic warfare, and spoofing effects [Brusak et al., 2024].

Based on the calculated coordinates, annual velocity vectors of displacement were determined in the coordinate directions V_N (north) and V_E (east). The coordinates were transformed into the ETRF-2020 reference frame to ensure compatibility with the motion of the European Tectonic Plate. Detailed station graphs and statistics are provided in the study [Tretyak et al., 2025]. Typical velocity values for the region, reflecting large-scale plate movements, were defined. As these vectors dominate the signal, correction was applied by subtracting the maximum velocity components along each axis. This approach proved effective at detecting millimeter-scale displacements, which are typical of slow geodynamic processes, and is particularly relevant for monitoring the stability of large hydraulic structures in geologically complex, seismically active regions. Table 1 presents the annual GNSS CORS velocities near the Dnister Hydropower Complex.

Table 1. Annual velocities of GNSS CORS near the Dnister Hydropower Complex

GNSS station	Annual velocity, mm/year ETRF-2020			Accuracy, mm	
	V_N	V_E	V_L	mV_N	mV_E
NDNS	–1.1	–1.7	2.0	0.1	0.1
RALI	–1.7	–2.0	2.6	0.1	0.1
VOVK	–1.1	–1.7	2.0	0.1	0.1
YAMP	–5.0	–2.3	5.5	0.2	0.1
KLMN	–1.8	–0.7	2.0	0.1	0.1
TULC	–0.1	–0.6	0.6	0.1	0.1
VINK	–0.0	–0.5	0.5	0.1	0.1
VINT	0.2	–0.4	0.4	0.1	0.0
VRBK	–5.2	–3.8	6.4	0.2	0.2

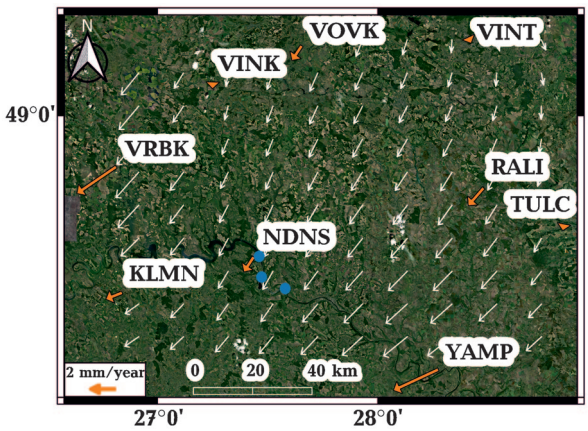

Fig. 1. The map of annual velocities of GNSS CORS (orange) and a model of a condensed vector field (white) of geodynamic deformations around the Dnister Hydropower Complex (blue circles).

Based on the obtained values, a dense vector model of the horizontal displacement velocities of the GNSS stations was constructed, reflecting local deformation processes within the study area. This map is presented in Fig. 1.

As shown in Fig. 1, the identified natural seismicity based on GNSS CORS data exhibits heterogeneous geodynamic characteristics. In the western part of the region, which is underlain by the more stable crystalline basement of the Ukrainian Shield, the natural deformation field is minimal and falls within the margin of measurement error. In contrast, in the southeastern part of the region, the deformation vectors increase up to 5 mm/year. This area hosts the main structures of the Dnister HPP and, as previously mentioned, is also seismically active. It is noteworthy that even such straightforward comparisons reveal a clear relationship within the system: recent geodynamics of the territory and seismicity.

Seismic Features of the territory. Instrumental observations of earthquakes in the region began in 1961. Until 2004, the regional seismic station network could detect only earthquakes with a local magnitude (ML>2.0). Consequently, during the filling of the reservoir, many weak seismic events in the area of the Complex went unrecorded due to the lack of seismic stations. Currently, three seismic stations are operating in close proximity to the Dnister HPP. These stations belong to the Carpathian regional seismic network [Verbytskyi et al., 2019; Pronyshyn et al., 2024, 2025]. At present, a seismic monitoring network consisting of 23 permanent seismic stations operates in the Carpathian region. The digital seismic stations of the Carpathian Seismological Network and the main technical parameters of the instruments that recorded seismic events are provided in Table 2.

The «Novodnistrovsk» seismic station has been operating in the vicinity of the Complex since 2006. Nearby stations also include «Kamenets-Podilskyi» (since 2005) and «Medzhybizh» (since October 2021; situated 30 km east of Khmelnytskyi). All stations are equipped with digital tools developed by the Seismicity Department of the Carpathian Region at the Institute of Geophysics of the National Academy of Sciences of Ukraine. At all stations, events were recorded along three components: N-S (North-South), E-W (East-West), and Z (Vertical).

Observations were processed according to the methodology outlined in the Instruction [Pronyshyn et al., 2024, 2025]. To determine the dynamic characteristics, amplitude-frequency response data of the channels in PAZ GSE1 format were used. To process and interpret the digital recordings, we applied several frequency filters and corrections for the instruments' amplitude-frequency transfer functions. This allows to detect relatively weak seismic events. The digital format of recordings enables direct storage in the database. To reliably identify indistinct or noise-contaminated seismic phases, a Butterworth band-pass filter (0.5—15 Hz) was used during the processing and interpretation of digital data. The choice of filter parameters depends on the quality (signal-to-noise ratio) and the spectral characteristics of the analyzed signal.

To calculate the energy characteristics of seismic events, the signal spectrum was corrected using the instrument's amplitude-frequency response and then converted into ground motion units. For this purpose, the amplitude-frequency response and sensitivity (in units of velocity, μm/s) were individually calculated for each seismic channel. To determine the main parameters — origin time, coordinates, and hypocentral depths, as well as

Table 2. Equipment and technical characteristics of digital seismic stations of the Carpathian Seismological Network

Number	Station name (year of establishment)	*H*, m	Coordinates		Equipment specifications			
			φ°N	λ°E	Equipment type	Dynamic range	Frequency range	Sensitivity count, μm/sec
1	Lviv LVV (1899)	320	49.820	24.031	Guralp CMG-40T	140	0.03—12	$0.8 \cdot 10^{-9}$
2	Morshyn MORU (1978)	260	49.124	23.876	DAS-05 CM3	120	0.2—15	—
3	Uzhhorod UZH (1934)	160	48.629	22.291	DAS-05 СКД	120	0.2—15	$1.05 \cdot 10^{-9}$
4	Mizhhiria MEZ (1961)	460	48.514	23.514	DAS-05 СКД	120	0.02—15	$9.6 \cdot 10^{-10}$
5	Trosnyk TRSU (1987)	120	48.095	22.957	DAS-05 CM-3KB	120	0.2—15	$2.05 \cdot 10^{-10}$
6	Nyzhne Selishche NSLU (1987)	250	48.198	23.457	DAS-05 CM-3KB	120	0.2—15	—
7	Rakhiv RAK (1956)	460	48.036	24.173	DAS-05 СКД	120	0.02—15	$4.98 \cdot 10^{-10}$
8	Kosiv KSV (1961)	450	48.314	25.065	DAS-04 СКД	120	0.02—15	$6.64 \cdot 10^{-10}$
9	Chernivtsi CHRU (1907)	300	48.298	25.922	DAS-05 СКД	120	0.02—15	$1.27 \cdot 10^{-9}$
10	Horodok HORU (1991)	340	49.214	26.426	DAS-05 CM-3	120	0.2—15	—
11	Korolev KORU (1998)	160	48.157	23.134	DAS-05 CM-3KB	120	0.2—15	$1.05 \cdot 10^{-10}$
12	Mukachevo MUKU (1999)	125	48.454	22.687	DAS-05 CM-3KB	120	0.2—15	$1.17 \cdot 10^{-10}$
13	Berehove BERU (2000)	160	48.234	22.646	DAS-05 CM-3	120	0.2—15	—
14	Brid BRIU (2000)	180	48.338	23.020	DAS-05 CM-3KB	120	0.2—15	$1.85 \cdot 10^{-10}$
15	Kamenets-Podilskyi KMPU (2005)	121	48.563	26.460	DAS-05 СКД	120	0.02—15	—
16	Novodnistrovsk NDNU (2006)	242	48.595	27.366	DAS-05 CM-3KB	120	0.2—15	$3.04 \cdot 10^{-10}$
17	Skhodnytsia SHIU (2006)	600	49.225	23.359	DAS-05 CM-3	120	0.2—15	$6.98 \cdot 10^{-10}$
18	Starunya STNU (2007)	391	48.710	24.502	DAS-05 CM-3	120	0.2—15	—
19	Stuzhytsia STZU (2011)	385	49.016	22.623	DAS-05 CM-3KB	120	0.2—15	$1.84 \cdot 10^{-10}$
20	Cholmec HOLU (2014)	134	48.527	22.384	DAS-05 CM-3KB	120	0.2—15	—
21	Lyubeshka LUBU (2019)	355	49.599	24.378	DAS-05 CM-3KB	120	0.03—12	$1.84 \cdot 10^{-10}$
22	Berezhany BRZU (2021)	292	49.457	24.951	DAS-05 CM-3KB	120	0.03—12	$1.84 \cdot 10^{-10}$
23	Medzhibizh MDZU (2021)	276	49.437	27.412	DAS-05 CM-3KB	120	0.03—12	$1.84 \cdot 10^{-10}$

the residuals of solutions and dynamic characteristics — additional seismic data from the national services of Moldova, Romania, Slovakia, Poland, and Hungary were also used.

During the comprehensive earthquake data processing at the stations, the following energy parameters of the recorded seismic events were determined:

– the seismic-energy class K_P according to the T.G. Rautian scale;

– the local magnitude *ML* according to the Richter scale, based on the maximum amplitude of the vertical component $A_{z\,max}$, calculated using the following formula:

$$ML = \lg(A_{z\,max}) - \lg(A_0); \quad (1)$$

– the magnitude *MSH* calculated from the amplitude of the *S*-wave A_S at the epicentral distance Δ, using the formula:

$$MSH = \lg A_S + 1.32\lg(\Delta, \mathrm{km}), \quad (2)$$

with a correction of +0.8 for intermediate-depth earthquakes in the Vrancea zone with $h \geq 70h$ km;

– the magnitude *MD* based on the signal duration *D* is determined using the A.S. Malamud formula:

$$MD = 2.67\lg(D, \mathrm{sec}) + 1.65. \quad (3)$$

This value is subsequently converted into the seismic-energy class (assuming $KD=K_P$) using the equation proposed by T.G. Rautian:

$$KD = 1.8MD + 4.0. \quad (4)$$

Fig. 2 summarizes the annual distribution of the number of earthquakes *N* and the logarithm of the total seismic energy *E* in joules (lg(Σ*E*)) released in the area of the Complex from 2012 to 2023. In terms of the number of earthquakes, there were four peak years, namely 2014, 2015, 2016, and 2022, when more than 100 earthquakes were recorded. The logarithm of the total seismic energy *E* in joules released in the region initially increases gradually from lg(Σ*E*)=7.5 in 2012 to lg(Σ*E*)=10 in 2016, and then decreases gradually according to a linear law from lg(Σ*E*)=10 in 2016 to lg(Σ*E*)=7 in 2023.

The epicenters of recorded earthquakes over the past decade in the region of the Complex are predominantly concentrated near the Dnister HPP and the main Dnister Reservoir. Therefore, we will focus more specifically on this region in further analysis. The causes of

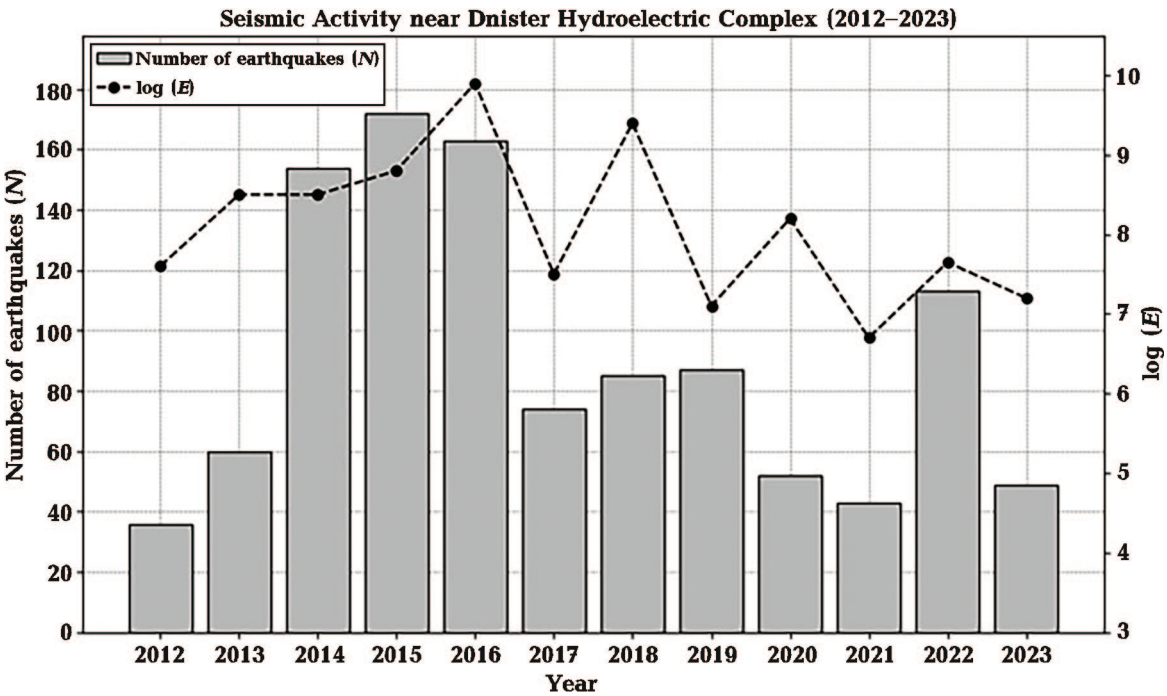

Fig. 2. The distribution of the earthquakes number *N* and the logarithm of the total seismic energy *E* in joules (lg(Σ*E*)) released in the area of the Complex during 2012—2023.

these earthquakes include both natural factors, since the area is intersected by tectonic faults [Sarnavski, Ovsiannikov, 2005], and the induced (triggered) seismicity [Zyhar et al., 2023; Tretyak et al., 2024b] related to the artificial regulation of the Dnister HPP dam. These low-magnitude earthquakes typically range from 0.1 to 1.3, with hypocenters at approximately 2 km depth. In view of this, we further consider reservoir water level fluctuations as a contributing factor to seismicity.

Changes in the water level in Dnister Reservoir. Archival data on the water level of the upper reservoir of the Dnister HPP were obtained directly from Ukrhydroenergo [2025] upon request. These records consist of automatic hourly measurements of the reservoir water level but are not systematically collected. Over the past decade, the lowest recorded water level was in 2015 at 112.92 meters, while the highest was in 2018 at 121.62 meters. The difference between the maximum and minimum levels during this period is 8.70 meters, which corresponds to a pressure change of approximately 85 kPa at the bottom of the reservoir. The average water level over these years is 118.56 meters.

When earthquakes in the region are plotted alongside water level graphs, it becomes challenging to identify clear patterns [Zyhar et al., 2023; Tretyak et al., 2024b]. To address this issue, we used machine learning techniques to detect underlying patterns in these datasets. A comprehensive machine learning-based approach was developed to analyze the interconnections between geodynamics and seismic activity in the area, considering fluctuations in the reservoir's water level. To explore the complex, nonlinear relationships among crustal deformations, the reservoir's hydrological regime, and seismic events, a multi-step approach involving three sequential machine learning algorithms was designed and implemented in Python with Scikit-learn library [Pedregosa et al., 2011]. The objectives of this methodology were not only to establish correlations but also to identify key predictor variables and classify earthquakes based on the behavioral patterns of these parameters.

The developed algorithm consists of three key stages.

1. Building a Random Forest predictive model to identify days with an increased probability of seismic events and determine the most influential factors.

2. Using Isolation Forest to generate an additional feature — the presence of anomalies in geodetic data, which improves the quality of the predictive model.

3. Clustering DBSCAN (Density-Based Spatial Clustering of Applications with Noise) behavior patterns to analyze and interpret scenarios preceding different types of earthquakes.

Such a sequential analysis allows us to move from raw data to conclusions about the nature of seismicity in the Complex.

Overall picture of correlations. The initial analysis identified numerous temporal coincidences between seismic events and anomalies in GNSS and water level data. All recorded events are visualized on a comprehensive timescale (Fig. 3), facilitating an overall assessment of the process dynamics. According to the correlation table, of 81 unique seismic events analyzed, 31 (38 %) coincided with either a GNSS anomaly or a significant change in water level within a 10-day window. This proportion is substantial and suggests a strong connection that extends beyond mere chance coincidences.

Fig. 3 confirms that seismic activity frequently occurs during periods of abnormal fluctuations in both the crust and the hydrological regime, suggesting a potential correlation. For instance, increased seismic activity in 2021 coincides with significant water level variations and notable anomalies in GNSS data. This pattern supports the hypothesis that the lithosphere-hydrosphere system in this region is closely interconnected, and disturbances in one component can trigger responses in the other.

Initially, the predictive modeling was performed, and the significance of the features was assessed. The first stage involved a binary classification task: training the model to recognize whether an earthquake would occur on a given day. The target variable (Y)

was a time series in which 1 corresponded to the earthquake dates s and 0 to days without seismic events. To build the model, a 'metrics laboratory' was created, within which a large set of derived features (X) was generated based on raw data (GNSS coordinates, water level). These features included:

– different averaging periods and water level lags;

– water level change rates and accelerations;

– statistical characteristics of time series (moving averages, standard deviations);

– geodynamic parameters (velocities, accelerations of GNSS station displacements).

As an additional feature, the result of the Isolation Forest algorithm was used [Hariri et al., 2021], which identified days with anomalous behavior of vertical displacements of the GNSS station [Brusak et al., 2025]. The inclusion of this feature (is_height_anomaly) improved the overall forecast quality by an average of 10 %. The Random Forest ensemble method was used to train the classifier. The results showed that the developed model is capable of predicting days with seismic activity with an F1-score accuracy in the range of 58—62 % and an F0.5-score accuracy of 45—55 %. The most important result of this stage was the ranking of features according to their impact on the forecast (Feature Importance). This made it possible to objectively identify the key factors preceding seismic events. The list of the most important features included:

– water_level (WL_t) — absolute water level in the Dnister Reservoir (average per day);

– wl_roll_mean_240d ($WL_t(240)$) — long-term average water level for the last 240 days;

– wl_lag_240d (WL_{t-240}) — water level value with a lag of 240 days, i.e., the difference between today's value and the value 240 days ago;

– wl_lag_60d (WL_{t-60}) — water level value with a lag of 60 days;

– wl_roll_std_90d ($\sigma_t(90)$) — standard deviation of water level over 90 days;

– is_height_anomaly — anomaly feature from Isolation Forest [Brusak et al., 2025];

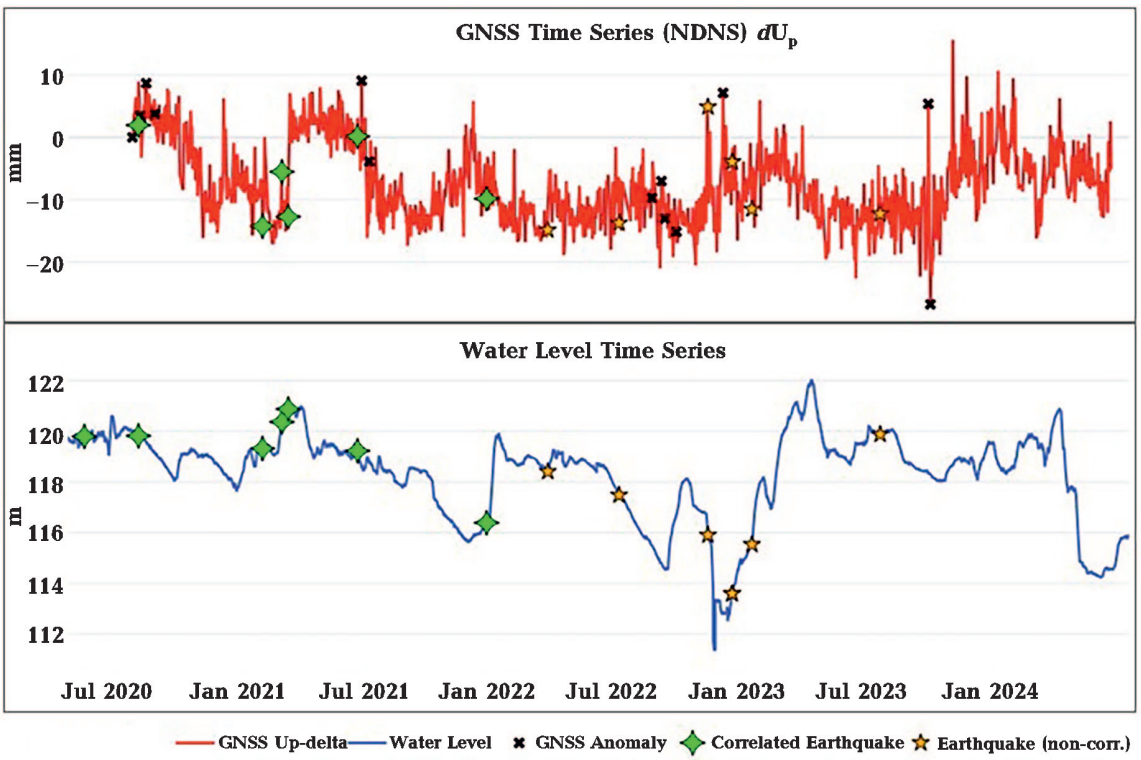

Fig. 3. Comprehensive time scale showing vertical displacements of the NDNS GNSS station (red line), water level in the reservoir (blue line), GNSS anomalies (black «x»), correlating (green rhombus) and non-correlating (orange stars) earthquakes.

– Up-delta (ΔU) — current displacement of Up component of GNSS station;

– Up-delta.mm_velocity (V_u) — vertical displacement velocity of Up component of GNSS station.

The presence of both hydrological and geodynamic parameters in this list confirms the complexity of the processes that lead to earthquakes in the region. Next, clustering of behavior patterns and differentiation of seismicity were carried out. After identifying the most important features, the next step was to study their collective behavior immediately before earthquakes. If we simply average the time series of all 81 events, as shown in Fig. 4, the individual patterns cancel each other out, and the overall picture appears noisy and uninformative. This highlights the need to use clustering to identify hidden groups with similar dynamics.

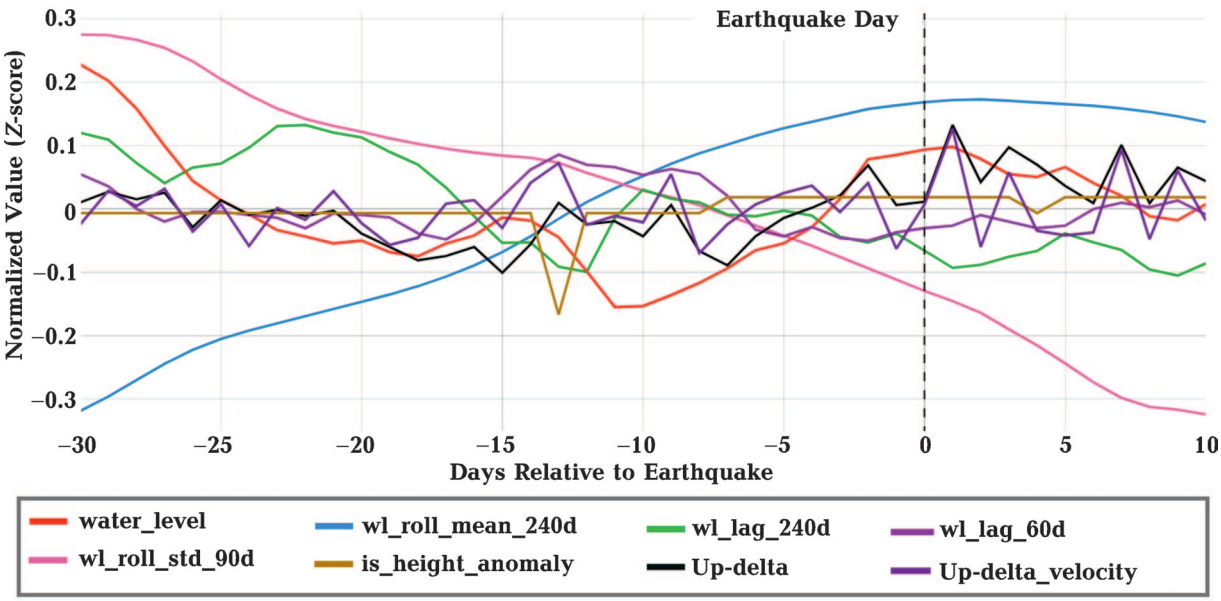

Fig. 4. Average behavior of key features for all seismic events.

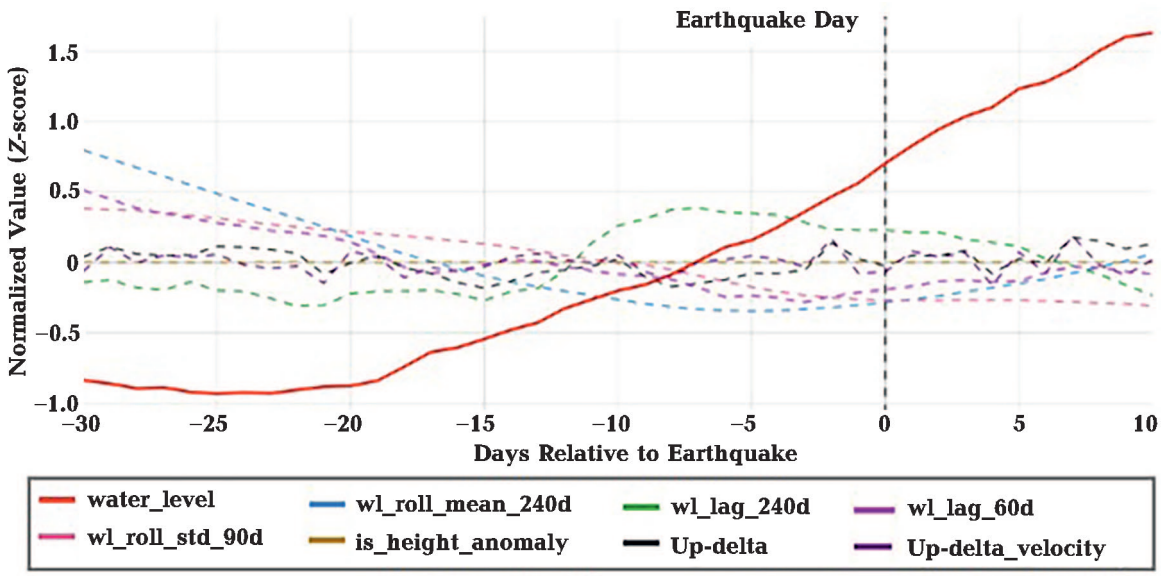

Fig. 5. Average behavior of features for the 'loading' cluster (28 events) based on the water_level feature.

Fig. 4 shows that, based on the parameters we have selected, it is difficult to differentiate events by probable causes when considering all events. However, it is interesting to note that 10 days before the earthquake, there is an intersection of the blue curve, which characterizes the average water level rise over 240 days, and the pink curve, which at the same time characterizes a decrease in the accuracy of the water level over the last 60 days.

The purpose of this stage was to group events according to similar preparation scenarios, which allows them to be differentiated by their probable mechanisms of occurrence. For this purpose, the DBSCAN density-based clustering algorithm was used. For each seismic event, a time window (30 days before and 10 days after) was taken with data on 9 key metrics. DBSCAN grouped these multidimensional time series based on the similarity of

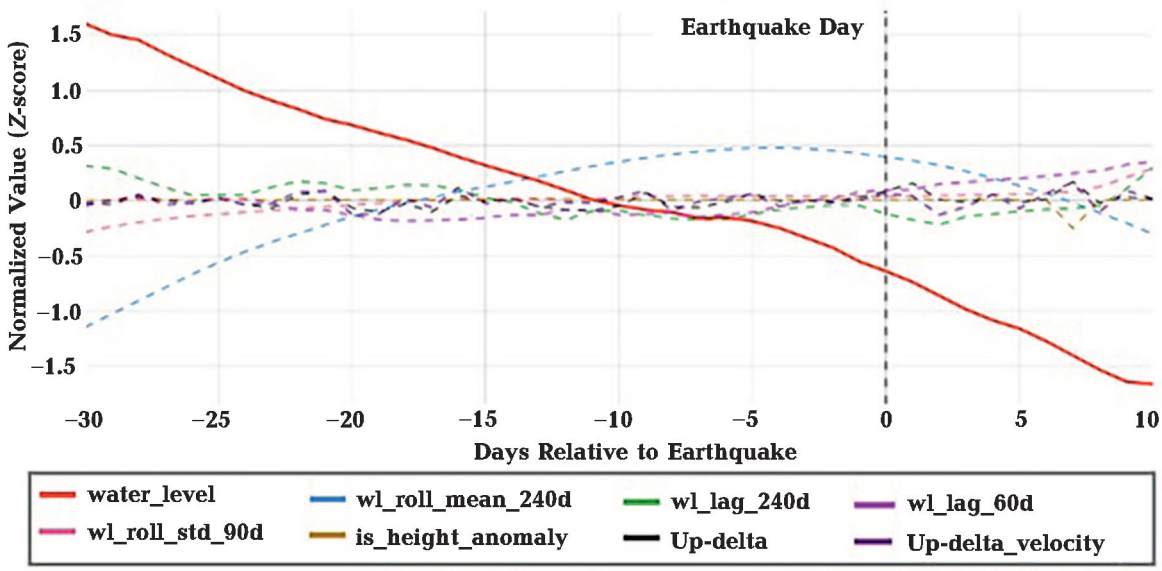

Fig. 6. Average behavior of features for the 'unloading' cluster (25 events) based on the water_level feature.

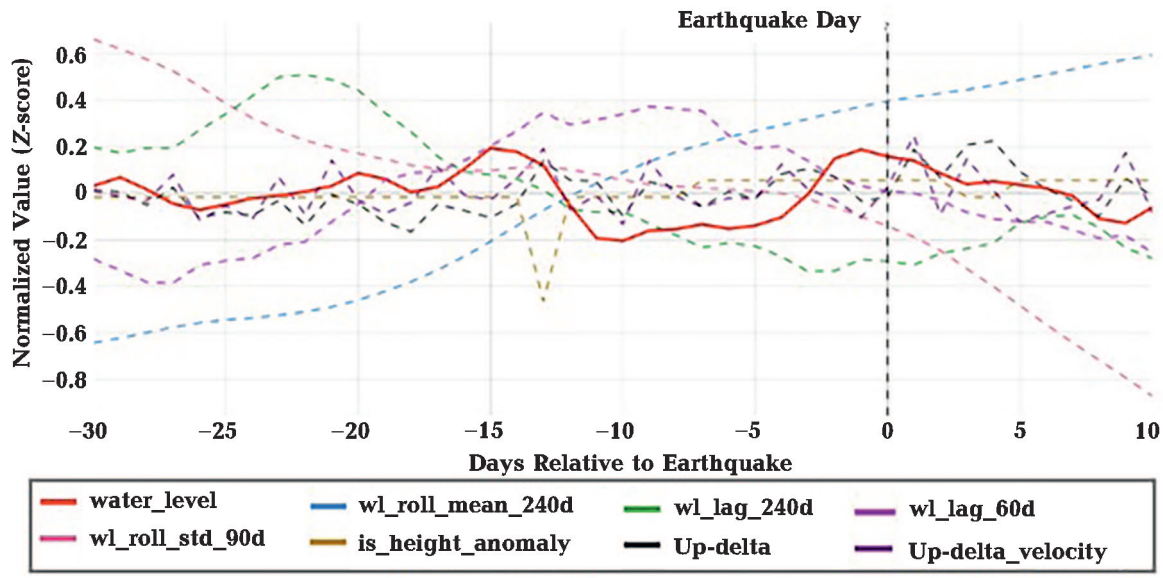

Fig. 7. Average behavior of features for the 'noise' events based on the water_level feature.

their shape, which allowed us to identify two stable clusters and a 'noise' group.

Analysis based on short-term changes in the water level (water_level). In the first stage, clustering focused on the water_level feature, which reflects the direct influence of hydrostatic pressure. In total, three clusters were identified: loading, unloading, and natural background. The first cluster, 'loading', includes 28 events. As shown in Fig. 5, this largest cluster is characterized by a clear and stable increase in the absolute water level (water_level) over the 20—25 days preceding the earthquake. This is likely a pattern of induced seismicity, where a gradual increase in hydrostatic load and the diffusion of pore pressure deep into the array act as triggers.

The next cluster, 'unloading', exhibits the opposite behavior (Fig. 6). It is preceded by a prolonged and significant decrease in the water level for 25 events. This scenario is another physically plausible mechanism for induced seismicity, where a reduction in the load on the reservoir bed leads to a decrease in the normal stresses that 'clamp' the fault.

The last group includes events that did not show consistent similarity to any of the two clusters (Fig. 7). The behavior of key features here is chaotic, with no clear trends. This gives good reason to assume that these earthquakes are predominantly of natural tectonic origin.

The results of the analysis of short-term changes in water level (*water_level*) are also shown on the map below. Fig. 8 illustrates the groups identified by their rapid response to hydrostatic pressure: 'loading' (blue) and 'unloading' (purple).

Analysis based on long-term water level trends (wl_roll_mean_240d). Since the long-term average of water level (wl_roll_mean_240d) was also identified as a key feature, additional clustering was performed to identify patterns associated with long-term hydrological cycles. This analysis provided insight into groups of events, highlighting scenarios that unfold over many months.

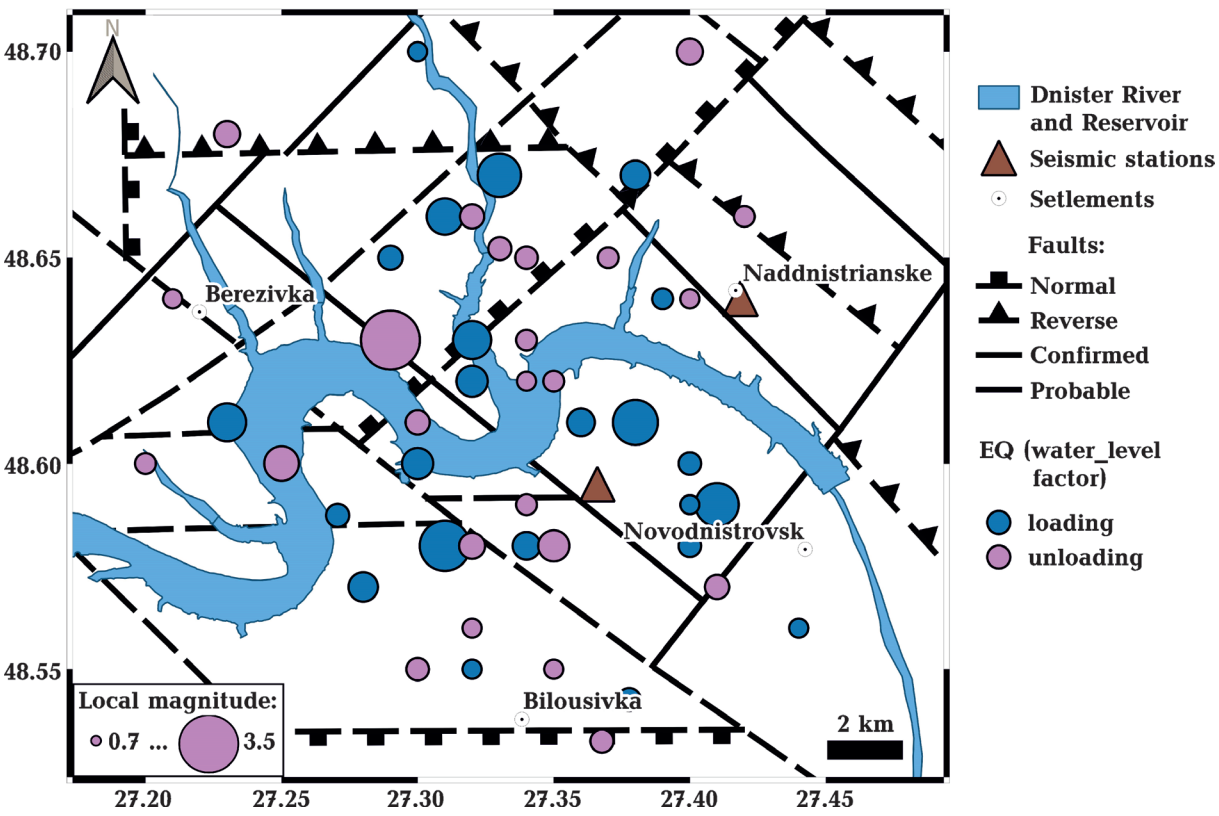

Fig. 8. Spatial distribution of clusters based on the water_level feature.

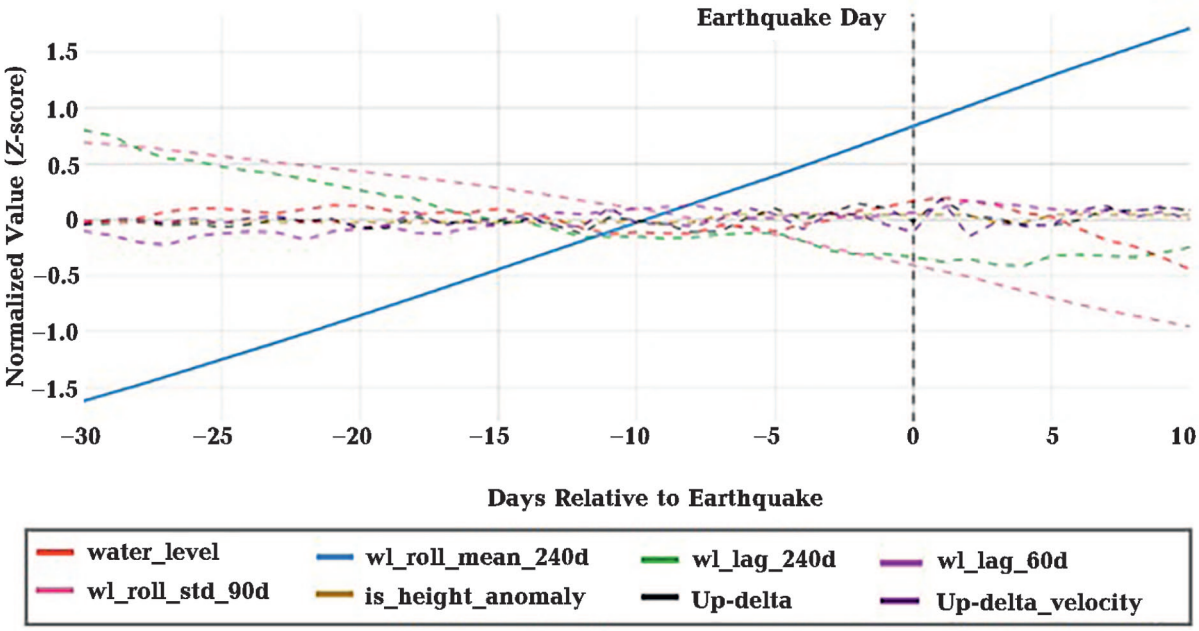

Fig. 9. Average behavior of features for cluster 'long-term loading' (29 events) based on the wl_roll_mean_240d feature.

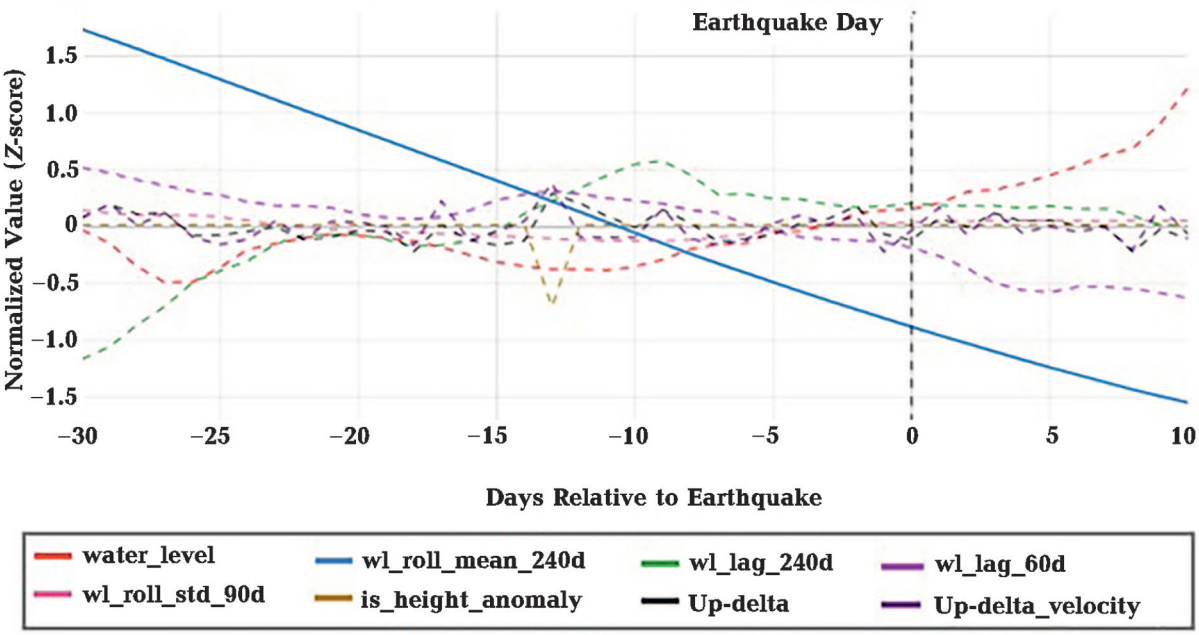

Fig. 10. Average behavior of features for the 'long-term unloading' cluster (18 events) based on the wl_roll_mean_240d feature.

This cluster is characterized by a steady, almost linear increase in the long-term mean water level over the 30-day period prior to the earthquake. This indicates that the seismic event occurs at the peak of a prolonged period of water accumulation in the reservoir. This pattern points to a mechanism in which it is not a short-term surge, but a prolonged, gradual increase in the load on the crust that plays an important role, slowly changing the stress state in the faults to a critical level. Fig. 9 shows the average behaviour of features for cluster 'long-term loading' (29 events) based on the wl_roll_mean_240d feature.

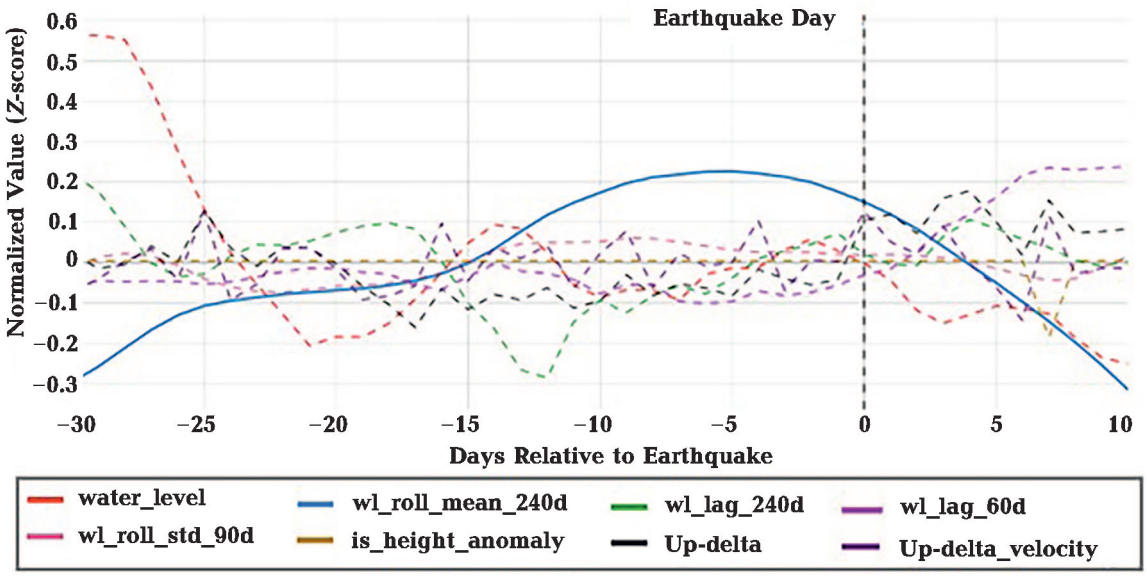

Fig. 11. Average behavior of features for the 34 'noise' events based on the wl_roll_mean_240d feature.

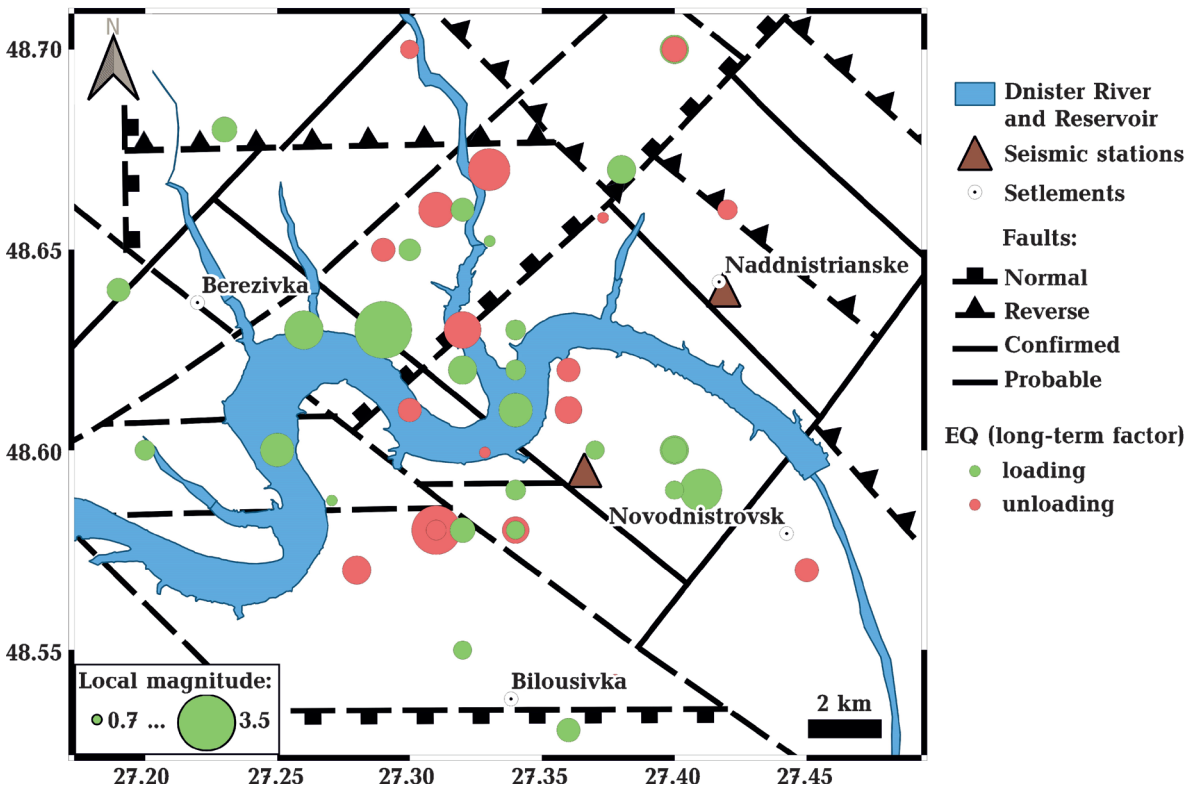

Fig. 12. Spatial distribution of clusters based on wl_roll_mean_240d.

Unlike the previous cluster, this one shows a steady, prolonged decrease in the average water level. The event occurs against the backdrop of a long-term 'unloading' of the reservoir. This may correspond to a scenario in which a prolonged decrease in water pressure destabilizes faults that were previously in a stable state under the weight of the water. Interestingly, against the backdrop of a general decline in wl_roll_mean_240d, there are

slight fluctuations in the current water level (water_level), suggesting a complex interaction between short- and long-term effects. Fig. 10 demonstrate the average behaviour of features for cluster 'long-term unloading' (18 events) based on the wl_roll_mean_240d feature.

The last group includes noise events for which no clear long-term trend has been identified. It could be transient processes or natural background. Average behavior of these 34 events is shown on Fig. 11.

Fig. 12 shows the distribution of events associated with long-term hydrological cycles: 'Long-term loading' (green) and 'Long-term unloading' (red).

Conclusions and discussion. This study examines seismic activity and geodynamic characteristics in the area surrounding the Dnister Hydropower Complex for the last decade. In the first stage, time series from nine GNSS stations in the GeoTerrace and SystemNet networks were analyzed from 2019 to 2024. Analysis of data from GNSS CORS stations in the region indicates that annual velocities have increased by nearly 2 mm per year, reflecting geodynamic deformations around the Dnister Hydropower Complex that coincide with an active seismic zone. It can also be noted that geodynamic activity, i.e., the annual velocities of GNSS stations, increases from the north-west from 1 mm/year to 3—4 mm/year, which corresponds to regions with higher seismic hazard.

The paper also provides details on the equipment and technical specifications of the digital seismic stations within the Carpathian Seismological Network, as well as the distribution of the number of earthquakes and the logarithm of the total seismic energy released in joules in the vicinity of the Dnister Hydropower Complex from 2012 to 2023. Regarding the earthquake frequency, four peak years were identified: 2014, 2015, 2016, and 2022, during which more than 100 earthquakes were recorded. The logarithm of the total seismic energy released in the region, measured in joules, initially exhibits a gradual increase from $\lg(\Sigma E)$=7.5 in 2012 to $\lg(\Sigma E)$=10 in 2016. Subsequently, it shows a steady decline following a linear trend from $\lg(\Sigma E)$=10 in 2016 to $\lg(\Sigma E)$=7 in 2023.

Next, we examined two potential factors that could influence seismicity: geodynamic factors derived from data collected at the nearby GNSS station NDNS and variations in the reservoir water levels. No evident correlation was observed between the GNSS deformation factor and earthquake occurrences. However, by applying machine learning techniques and the DBSCAN clustering method, we were able to identify meaningful clusters based on this information. The established correlations indicate a probable connection between changes in water pressure in the reservoir and the number and energy of earthquakes in the Dnister Reservoir area. It is clear that this connection is not clearly expressed mathematically. However, it allows us to conclude that changes in the water level of the Dnister Reservoir affect local seismic activity.

To evaluate whether different earthquake mechanisms are linked to specific geological structures, a spatial analysis of the identified clusters was conducted. The application of clustering to features with varying time scales (water_level and wl_roll_mean_240d) enables the differentiation of seismic events not only by immediate triggers such as rapid loading or unloading but also by background conditions accumulated over several months. This suggests a complex nature of induced seismicity in the Dnister Hydropower Complex area. A key and consistent finding from both analyses is the lack of distinct spatial segregation between clusters. Whether triggered by sudden water level changes or long-term trends, seismic events appear randomly distributed across the study region, primarily concentrating along the reservoir bed. This fundamental observation indicates that the same fault zones are responsive to different types of trigger effects. The occurrence of earthquakes triggered by both rising and falling water levels across different time scales in the same locations points to a critically stressed state of the local geological structures. The lithosphere-hydrosphere system in this region is highly sensitive, where any

significant change in stress — regardless of its direction or duration — can activate pre-existing faults, leading to seismic events.

Acknowledgements. The research was carried out within the framework of the DB/GEOS project «Analysis of the Impact of Military Operations on Spatial Deformations of the Dnister Hydropower Complex Using Contact and Remote Methods» (No. 0125U000496).

References

Brusak, I., Babchenko, V., Savchuk, N., Marchuk, V., Shkvarok, Y., & Turianytsia, M. (2024). New challenges for exploitation of continuously operating reference GNSS stations during hostilities. Case study of Ukraine. *Geodesy, Cartography and Aerial Photography*, (99), 28—37. https://doi.org/10.23939/istcgcap2024.99.028.

Brusak, I., Maciuk, K., & Haidus, O. (2025). Detection of geodynamic anomalies in GNSS time series using machine learning methods. *Geodynamics, 1*(38), 37—48. https://doi.org/10.23939/jgd2025.01.037.

Brusak, I., Tretyak, K., & Pronyshyn, R. (2022). Preliminary studies of seismicity caused by the water level changes in Dnister upper reservoir. *International Conference of Young Professionals «GeoTerrace-2022»* (pp. 1—4). https://doi.org/10.3997/2214-4609.2022590022.

DBN V.1.1-12:2014. Construction in the seismic regions of Ukraine. (2014). Kyiv: Ministry of Regional Development of Ukraine (in Ukrainian).

Doskich, S., Savchuk, S., & Dzhuman, B. (2023). Determination of horizontal deformation of the Earth's crust on the territory of Ukraine based on GNSS measurements. *Geodynamics, 2*(35), 89—98. https://doi.org/10.23939/jgd2023.02.089.

Fazilova, D., Makhmudov, M., & Khalimov, B. (2025). The analysis of crustal deformation patterns in the Tashkent region, Uzbekistan, derived from GNSS data over the period 2018–2023. *Geodesy and Geodynamics*, *16*(2), 137—146. https://doi.org/10.1016/j.geog.2024.07.001.

Hurskyi, D.S., & Kruglov, S.S. (Eds.). (2007). *Tectonic map of Ukraine.1:1000 000*. Kyiv: Publ. of the Ukrainian State Geological Prospecting Institute, 95 p. (in Ukrainian).

Hariri, S., Kind, M., & Brunner, R. (2021). Extended isolation forest. *IEEE Transactions on Knowledge and Data Engineering, 33*(4), 1479—1489. https://doi.org/10.1109/TKDE.2019.2947676.

Kao, H., Hyndman, R., Jiang, Y., Visser, R., Smith, B., Babaie Mahani, A., Lucinda, L., Hadi, G. & He, J. (2018). Induced seismicity in western Canada linked to tectonic strain rate: Implications for regional seismic hazard. *Geophysical Research Letters, 45*(20), 1—12. https://doi.org/10.1029/2018GL079288.

Naumowicz, B., Kowalczyk, K., & Pelc-Mieczkowska, R. (2024). PPP Solution-based model of absolute vertical movements of the Earth's crust in Poland with consideration of geological, tectonic, hydrological and mineral information. *Earth and Space Science, 11*(12), e2023EA003268. https://doi.org/10.1029/2023EA003268.

Pedregosa, F., Varoquaux, G., Gramfort, A., Michel, V., Thirion, B., Grisel, O., Blondel, M., Prettenhofer, P., Weiss, R., Dubourg, V., Vanderplas, J., Passos, A., Cournapeau, D., Brucher, M., Perrot, M., & Duchesnay, E. (2011). Scikit-learn: Machine learning in Python. *Journal of Machine Learning Research, 12*, 2825—2830. https://doi.org/10.48550/arXiv.1201.0490.

Pospisil, L., Bartonek, D., Hefty, J., & Machotka, R. (2019). Geodetic Signs of the Recent Kinematical and Geodynamical Deformation of the Carpathian Arc. *IOP Conference Series: Earth and Environmental Science* (Vol. 221, No 1, p. 012001). https://doi.org/10.1088/1755-1315/221/1/012001.

Pronyshyn, R., Kuplovskyi, B., Prokopyshyn, V., Stetskiv, O., Nischimenko, I., Keleman, I., Gerasymenyuk, G., & Batiuk, A. (2024). Seismicity of the Carpathians in 2023. *Geofizychnyi Zhurnal, 46*(5), 82—92. https://doi.org/10.24028/gj.v46i5.309221 (in Ukrainian).

Pronyshyn, R., Kuplovskyi, B., Prokopyshyn, V., Stetskiv, O., Nischimenko, I., Keleman, I., Gerasymenyuk, H., & Batiuk, A. (2025). The seismicity of the Carpathians in 2024. *Geofizychnyi Zhurnal, 47*(5), 95—105. https://doi.org/10.24028/gj.v47i5.335308 (in Ukrainian).

Sarnavski, V., & Ovsiannikov, M. (2005). Tectonic structure and geodynamic mode of rock

masses in the zone of interaction with hydromechanical structures of HPP and PSPP (on the example of the Dnister complex hydro unit). In *Modern achievements of geodetic science and production* (pp. 193—206). Lviv: Publ. house of the National University «Lviv Polytechnic» (in Ukrainian).

Savchyn, I., & Pronyshyn, R. (2020) Differentiation of recent local geodynamic and seismic processes of technogenic-loaded territories based on the example of Dnister Hydro Power Complex (Ukraine). *Geodesy and Geodynamics, 11*(5), 391—400. https://doi.org/10.1016/j.geog.2020.06.001.

Sidorov, I., Perij, S., & Sarnavski, V. (2015). Determination of the earth surface movements in areas of Dnister PSPP using satellite and ground geodetic methods. *Geodynamics, 19*(2), 15—25. https://doi.org/10.23939/jgd2015.02.015 (in Ukrainian).

State geological map of Ukraine on scale of 1:200.000. sheets M-35-XXVIII (Bar). M-35-XXXIV (Mohyliv-Podilskyi (within Ukraine). (2007). Ministry of Environmental Protection of Ukraine. State Geological Service UkrDGRI, 206 p. (in Ukrainian).

Tretyak, K., Brusak, I., Savchuk, N., Kozak, A., & Babchenko, V. (2025). Geodynamic features of territories around Ukraine's hydroelectric power plants based on GNSS CORS data. *Geodynamics, 2*(39), 70—82. https://doi.org/10.23939/jgd2025.02.070.

Tretyak, K., Brusak, I., & Babchenko, V. (2024a). Recent deformations of the Earth's crust in Ukraine based on GNSS network data from Geoterrace and System.Net. *Geodynamics, 2*(37), 56—68. https://doi.org/10.23939/jgd2024.02.056.

Tretyak, K., Brusak, I., & Pronyshyn, R. (2024b). Reservoir-triggered seismicity: case study of the Dnister Hydro Power Complex (Ukraine). *Geofizychnyi Zhurnal, 46*(1), 38—51. https://doi.org/10.24028/gj.v46i1.298659.

Tretyak, K., & Romaniuk, V. (2018). The research of interrelation between seismic activity and modern vertical movements of the European permanent GNSS-stations. *Acta Geodynamics et Geomaterial, 15*(2), 143—164. https://doi.org/10.13168/AGG.2018.0010.

Ukrhydroenergo. (2025). Ukrhydroenergo — the leading hydropower company in Ukraine. Ukrhydroenergo. Retrieved from https://uhe.gov.ua/diyalnist/proekti.

Verbytskyi, S.T., Verbytskyi, Y.T., Stetskiv, O.T., & Nischimenko, I.M. (2019). Automated subsystem for processing and analyzing seismic data from the Carpathian region. *Geofizicheskiy Zhurnal, 41*(2), 171—181. https://doi.org/10.24028/gzh.0203-3100.v41i2.2019.164467 (in Ukrainian).

Wu, S., Ouyang, H., Li, H., Li, Z., Li, H., & He, Y. (2025). GNSS time series analysis of the crustal movement network of China: Detecting the optimal order of the polynomial term and its effect on the deterministic model. *Geodesy and Geodynamics, 16*(4), 378—386. https://doi.org/10.1016/j.geog.2024.12.002.

Zyhar, A., Yushchenko, Yu., & Savchyn, I. (2023). A study of the influence of water level fluctuations on the geodynamic situation in the natural and technical geosystem of the Dnister HPP and PSPP cascade. *Geodesy, Cartography and Aerial Photography,* (97), 24—31. https://doi.org/10.23939/istcgcap2023.97.024.

Застосування методів машинного навчання для вивчення взаємозв'язків сейсмічності та геодинамічних особливостей Дністровського гідроенергетичного комплексу

І.В. Брусак[1], О.А. Гайдусь[1], Б.Є. Купльовський[2], 2026

[1]Національний університет «Львівська політехніка», Інститут геодезії, Львів, Україна
[2]Відділ сейсмічності Карпатського регіону Інституту геофізики ім. С.І. Субботіна НАН України, Львів, Україна

Приведено результати досліджень сейсмічності та сучасних геодинамічних особливостей Дністровського гідроенергетичного комплексу в Україні з акцентом на застосуванні методів машинного навчання для аналізу їхніх взаємозв'язків. Дністровський гідроенергетичний комплекс, розташований у сейсмічно активній перехідній зоні, перебуває під впливом природних тектонічних процесів та антропогенної діяльності, зокрема експлуатації Дністровської гідроелектростанції та активних змін рівня води у Дністровському водосховищі. Зібрано та проаналізовано дані цифрових сейсмічних станцій Карпатської сейсмологічної мережі, перманентних станцій Глобальної навігаційної супутникової системи мереж GeoTerrace та SystemNet, а також записи рівня води в Дністровському водосховищі. Для виявлення закономірностей та кореляцій між деформаціями земної кори, коливаннями рівня води та сейсмічними подіями були застосовані алгоритми машинного навчання Random Forest, Isolation Forest та кластеризацію DBSCAN. Результати показують значний зв'язок між змінами рівня води — як короткостроковими, так і довгостроковими — та виникненням землетрусів, що свідчить про вплив гідрологічних змін на сейсмічну активність. Геодинамічний аналіз вказує на неоднорідні закономірності деформації з підвищеними швидкостями в сейсмічно активних південно-західних частинах регіону. Дані з перманентних станцій Глобальної навігаційної супутникової системи показують збільшення швидкостей приблизно на 2 мм/рік поблизу Дністерського гідроенергетичного комплексу. Сейсмічність поблизу комплексу з 2012 по 2023 р. характеризувалася піковими роками (2014—2016 та 2022), у кожному з яких зафіксовано понад 100 подій. Загальна вивільнена сейсмічна енергія зросла з $\lg(\Sigma E)=7{,}5$ у 2012 р. до 10 у 2016 р., а потім поступово знизилася до 7 у 2023 р. Ці висновки сприяють кращому розумінню механізмів індукованої сейсмічності, пов'язаної з експлуатацією водосховищ, і надають цінну інформацію для оцінювання ризиків і розробки стратегій їхнього зменшення в гідроелектричних регіонах. Інтегрований підхід демонструє ефективність машинного навчання в розшифровці складних геодинамічних і сейсмічних взаємодій у тектонічно чутливих середовищах.

Ключові слова: сейсмічність, сучасна геодинаміка, індукована сейсмічність, зміни рівня води, Дністровський гідроенергокомплекс, машинне навчання.